ADVANCED MATERIALS
www.advmat.de

Nonpersistent Nanoarchitectures Enhance Concurrent Chemoradiotherapy in an Immunocompetent Orthotopic Model of HPV+ Head/Neck Carcinoma

Alessandra Gonnelli, Marine Gerbé de Thoré, Maria Laura Ermini, Valentina Frusca, Agata Zamborlin, Nicolas Signolle, Olivia Bawa, Céline Clémenson, Lydia Meziani, Paul Bergeron, Ismail El-Azrak, Patrizia Sarogni, Enrico Mugnaioli, Noemi Giannini, Giuliana Drava, Eric Deutsch, Fabiola Paiar, Michele Mondini,* and Valerio Voliani**

Cisplatin chemoradiotherapy (CRT) is the established standard of care for managing locally advanced human papillomavirus-positive head/neck carcinoma. The typically young patients may suffer serious and long-time side effects caused by the treatment, such as dysphagia, and hearing loss. Thus, ensuring a satisfactory post-treatment quality of life is paramount. One potential replacing approach to the classical CRT involves the combination of standard-dose radiotherapy and radiosensitizers such as noble metal nanoparticles (NPs). However, several concerns about size, shape, and biocompatibility limit the translation of metal nanomaterials to the clinical practice. Here, it is demonstrated that a new model of nonpersistent gold nanoarchitectures containing cisplatin (NAs-Cluster-CisPt) generates, in combination with radiotherapy, a significant in vivo tumor-reducing effect compared to the standard CRT, achieving a complete tumor clearance in 25% of the immunocompetent models that persist for 60 days. These findings, together with the negligible amount of metals recognized in the excretory organs, highlight that the concurrent administration of NAs-Cluster-CisPt and radiotherapy has the potential to overcome some clinical limitations associated to NP-based approaches while enhancing the treatment outcome with respect to standard CRT. Overall, despite further mechanistic investigations being essential, these data support the exploiting of nonpersistent metal-nanomaterial-mediated approaches for oral cancer management.

1. Introduction

Among patients diagnosed with head and neck squamous cell carcinoma (HNSCC), a specific subgroup is characterized by high-risk human papillomavirus (HPV) infection. This subgroup exhibits distinct epidemiological, clinical, and molecular features. Extensive retrospective and prospective studies have consistently demonstrated that patients with HPV-positive HNSCC have significantly improved survival outcomes compared to HPV-negative.[1,2] Moreover, the HPV+ HNSCC survivors are typically young, thus ensuring a satisfactory post-treatment quality of life is paramount. Indeed, a notable portion of these patients encounter serious side effects from the treatment, such as xerostomia, dysphagia, neck discomfort, and hearing loss.[3] Hence, it is crucial to reduce the negative effects linked to the established gold standard treatments.[4]

Despite numerous ongoing studies investigating de-escalation strategies for the treatment of locally advanced HPV-positive

A. Gonnelli, M. L. Ermini, V. Frusca, A. Zamborlin[+], P. Sarogni[++], N. Giannini, V. Voliani
Center for Nanotechnology Innovation@NEST
Istituto Italiano di Tecnologia
Piazza San Silvestro 12, Pisa 56127, Italy
E-mail: valerio.voliani@unige.it

The ORCID identification number(s) for the author(s) of this article can be found under https://doi.org/10.1002/adma.202400949

[+]Present address: Ghent Research Group on Nanomedicines, Department of Pharmaceutics, Ghent University, Ottergemsesteenweg 460, Ghent B-9000, Belgium

[++]Present address: Molecular Modeling and Drug Discovery Lab, Istituto Italiano di Tecnologia, via Morego, 30, Genoa 16163, Italy

DOI: 10.1002/adma.202400949

A. Gonnelli, N. Giannini, F. Paiar
Radiation Oncology Unit
Pisa University Hospital "Azienda Ospedaliero-Universitaria Pisana"
Via Roma 67, Pisa 56126, Italy
E-mail: fabiola.paiar@unipi.it

M. Gerbé de Thoré, C. Clémenson, L. Meziani, P. Bergeron, I. El-Azrak, E. Deutsch, M. Mondini
Gustave Roussy
INSERM U1030 Molecular Radiotherapy and Therapeutic Innovation
Université Paris Saclay
114, rue Edouard Vaillant, Villejuif Cedex 94805, France
E-mail: michele.mondini@gustaveroussy.fr

V. Frusca
Scuola Superiore Sant'Anna
Piazza Martiri della Libertà 33, Pisa 56127, Italy

HNSCC, cisplatin-based chemoradiotherapy (CRT) is still the standard of care.[5–7] This highlights the existing gap in specific therapeutic options for managing HPV-related tumors. Nowadays, there are no alternative therapies that can effectively enhance the therapeutic ratio for these tumors. This objective can be achieved by integrating innovative approaches that enhance the therapeutic efficacy of radiotherapy while mitigating the associated toxicity. A potential alternative approach involves the combination of standard-dose radiotherapy with radiosensitizers, thereby amplifying the effectiveness of radiation therapy within tumor cells while minimizing damages to neighboring healthy tissues.[8]

In this context, the progressive application of metal nanoparticles (NPs) as radiosensitizers for the treatment of some carcinoma emerges as a promising strategy in preclinical exploration.[9] Notably, upon exposure to ionizing radiation, NPs intensify the radiation dose deposition within tumors owing to their elevated atomic number. This phenomenon, together with the increased accumulation of NPs in some neoplasms, results in an enhanced DNA damages and eradication of tumor cells.[10]

However, several concerns about the size, shape, and biocompatibility limit the translation of metal nanomaterials to the clinical practice.[11] To address the issue of metal persistence, our research team has developed a family of nanoarchitectures (NAs) that demonstrated promising excretion trends by following intravenous or intranasal administration in animal models.[12–14,15] This is due to the peculiar structure of NAs, which consist of polymeric aggregates of ultrasmall nanoparticles (USNPs) encapsulated within a biodegradable silica capsule of ≈150 nm.[12] This design combines an optimal overall size for intracellular uptake with useful optical properties and degradation kinetics, making NAs nonpersistent versatile platforms for oncological applications.[16,17] Nowadays, NAs have been preclinically investigated for their potential application in targeted drug delivery, chemo-/photothermal therapy, photoacoustic/ultrasound imaging, metastasis modulation, and as radiosensitizers.[18–20] In the latter, we evaluated the tumor growth delay in alternative in vivo models of pancreatic ductal adenocarcinoma (PDAC) in a chemoradiotherapy setting where ionizing radiation (IR) was administered concurrently with NAs, either plain or loaded with a cisplatin prodrug.[19] Despite the promising results of NAs as cisplatin delivery systems, the radiosensitizing effect associated to USNPs was limited. This can be attributed either to a nonoptimal size of the USNPs or to a low gold content (% w/w) in NAs. On the other hand, standard gold NAs have demonstrated comparable effects to free cisplatin in CRT in alternative in vivo models of HPV-negative HNSCCs.[21]

In the present study, a novel type of NAs (NAs-Cluster-CisPt) encapsulating gold clusters of about 1 nm (Au loading: 15% w/w) and cisplatin has been designed, produced, characterized, and explored. Orthotopic HPV+ HNSCC immunocompetent murine models have been employed to evaluate the effects of concurrent CRT mediated by NAs-Cluster-CisPt (and, as control, NAs-Cluster), and the efficacy compared to the gold standard treatment (i.e., cisplatin-mediated CRT). Our research confirmed the superior effectiveness of multimodal treatments compared to monomodal approaches and uncovered an interesting radiosensitizing effect of NAs-Cluster-CisPt that resulted in a significant tumor reduction compared to the standard strategies with a 60 days persistent tumor clearance in 25% of the models. These findings hold particular importance in HPV+ oral cancer management as our approach overcomes the clinical limitations associated to metal-nanoparticle-mediated radiotherapy while enhancing the treatment outcome with respect to the gold standard treatment, opening new horizons for the clinical employment of nonpersistent inorganic nanomaterials.

2. Experimental Section

2.1. Synthesis of Nanoparticles

2.1.1. Synthesis of Gold Clusters

Ultrasmall gold cluster nanoparticles of 1 nm in diameter were synthesized in a 50 mL plastic tube by first adding 200 µL of freshly prepared L-glutathione solution (GSH; aqueous solution, 100 mM, Sigma-Aldrich) and 200 µL of tetrachloroauric acid; (25 mM, Alfa Aesar) to 20 mL of Milli-Q water. Then, 200 µL of sodium borohydride; (211 mM, Sigma-Aldrich) was added in a single fast shot under vigorous stirring of the reaction mixture (1200 rpm). The solution turned from milky white to pale yellow. After a few minutes of rest, 8 µL of poly(sodium 4-styrene sulfonate) (PSS; 30% in water, 70 kDa, Sigma-Aldrich) was added. The reaction mixture was set to mix on an orbital shaker at 70 rpm for 10 min.

For CisPt-loaded cluster NPs (Cluster-CisPt), 2 mg of cisplatin (*cis*-diamineplatinum(II) dichloride; Sigma-Aldrich) was added before the addition of PSS by directly dissolving it in the reaction mixture.

2.1.2. Synthesis of Cluster and Cluster-CisPt Polymeric Arrays

Polymeric arrays of Cluster (or Cluster-CisPt) were formed by adding 175 µL of poly(ethylene imine) (PEI; 50% w/w aqueous solution, 5 µg mL^{-1}, M_n 1800, Sigma-Aldrich) to the reaction mixture from Section 2.1.1 and then shaking for 30 min on an orbital shaker (50 rpm). Polymeric arrays were gathered by centrifugation at 14 000 rpm for 4 min at room temperature, yielding a light brown precipitate. The supernatant was discarded, and the arrays were resuspended in 2 mL Milli-Q water by sonication.

A. Zamborlin[+]
NEST-Scuola Normale Superiore
Piazza San Silvestro 12, Pisa 56127, Italy
N. Signolle, O. Bawa
Gustave Roussy
Plateforme de pathologie expérimentale et translationnelle
UMS AMMICA
114, rue Edouard Vaillant, Villejuif Cedex 94805, France
E. Mugnaioli
Department of Earth Sciences
University of Pisa
Via S. Maria 53, Pisa 56126, Italy
G. Drava, V. Voliani
Department of Pharmacy
School of Medical and Pharmaceutical Sciences
University of Genoa
Viale Cembrano 4, Genoa 16148, Italy

2.1.3. Synthesis of NAs-Cluster and NAs-Cluster-CisPt

A silica shell (20 nm thick) was grown around the polymeric arrays according to a modified Stöber reaction protocol. 40 µL of tetraethyl orthosilicate (98%, Sigma-Aldrich) was added to 70 mL of pure ethanol (EtOH; Sigma-Aldrich) and allowed to mix for 1 min at room temperature. Then, 2 mL of the Cluster (or Cluster-CisPt) arrays from Section 2.1.2 was added. The new reaction mixture was shaken for 5 min, and 2.4 mL of ammonia solution (30% in water, Sigma-Aldrich) was added. The resulting mixture was incubated under gentle shaking for further 3 h on an orbital shaker at room temperature. NAs-Cluster (or NAs-Cluster-CisPt) were retrieved by centrifuging for 30 min at 4000 rpm at room temperature. A few washing steps were performed to remove any unreacted reagent by precipitation (3 min, 14 000 rpm) and the supernatant was replaced with fresh EtOH (1 mL). A short spin (15 s) was useful to eliminate bigger particles. The final product was stored in EtOH at −20 °C until use.

2.2. Nanoparticle Characterization

2.2.1. Transmission Electron Microscopy (TEM)

Transmission electron microscopy images were acquired either with a Zeiss Libra 120 operating at 120 kV accelerating voltage (NAs-Cluster), or with a JEOL JEM-F200 operating at a 200 kV accelerating voltage (NAs-Cluster-CisPt). The samples were prepared by dropping the ethanol suspension of NAs onto a 300-mesh carbon-coated copper grid and letting to dry before TEM acquisition. The images were processed with ImageJ to obtain the diameter and shell thickness of at least 100 nanoparticles.

2.2.2. Scanning Transmission Electron Microscopy (STEM) and Energy-Dispersive X-Ray (EDX) Spectroscopy

Scanning transmission electron microscopy images of both NAs-Cluster and NAs-Cluster-CisPt were acquired with a JEOL JEM-F200, working at 200 kV and equipped with a Schottky-field emission gun (FEG) source and high-counting silicon drift detector (SDD). EDX maps were performed in scanning mode, with a probe size of 4–6, and a counting time of 30 s (single EDX spot analysis) or 3 min (EDX maps). Samples were prepared as in Section 2.2.1. EDX spectra were acquired by using a region of interest (ROI) size of 80 nm × 80 nm.

2.2.3. Dynamic Light Scattering (DLS) and Zeta Potential

Dynamic light scattering and zeta-potential measurements were performed on a Malvern Zetasizer nano-ZS90 (Malvern Instruments, Malvern, UK) with a scattering angle of 90°. Samples were resuspended in 1 mL phosphate-buffered saline (PBS) 1 × (pH 7.4) and placed in quartz cuvettes for hydrodynamic diameter measurements via DLS or in DTS 1070 standard capillary cells for zeta-potential measurements. Values were the average result of three consecutive measurements.

2.2.4. Inductively Coupled Plasma-Mass Spectrometry (ICP-MS) Analysis

The metal (Au, Pt) elemental content of NAs-Cluster and NAs-Cluster-CisPt was evaluated via mass spectrometry on an Agilent ICP-MS 7700 (Agilent Technologies, Santa Clara, CA, USA). Aliquots of ethanol suspensions of NAs were placed in glass pressure vessels and added with 200 µL of aqua regia, freshly prepared by mixing hydrochloric acid (Trace Metal Grade, Thermo Fisher Scientific) and nitric acid (HNO_3; 65% Suprapur, Sigma-Aldrich) in a 3:1 ratio. Samples were digested at 200 °C under microwave irradiation using CEM Discover SP-D (CEM, Matthews, NC, USA) and then diluted in 3 mL of 3% HNO_3 solution. Quantification was performed by analysis against standard calibration curves (Au standard: 1000 ppm, Absolute Standards, Inc.; Pt standard: 1000 ppm, Absolute Standards, Inc.) using as internal standard a 10 ppm solution of Hg in 3% HNO_3 solution (10 000 ppm; Sigma-Aldrich). Values were the average result of three consecutive measurements.

2.2.5. Gold and Platinum Content Measurement

The ratio of gold and platinum content in NAs-Cluster and NAs-Cluster-CisPt was assessed as % w/w on dried NAs. NA aliquots containing 10 µg of Au were centrifuged at 14 000 rpm for 3 min to withdraw ethanol. Several spins followed to remove as much solvent as possible. NAs were then dried using SpeedVac Christ Rotary Vacuum Concentrator (RVC) 2–18 CD plus at 250 rpm, 36 °C at 50 mbar for 8 h. After weighting, dried NAs were placed in glass pressure vessels, added 200 µL aqua regia, and digested as described in Section 2.2.4. ICP-MS analysis performed as in Section 2.2.4 allowed to quantify the metal content in NAs, which was used to calculate the percentage ratio of µg metal/µg NAs (% w/w).

2.2.6. UV–Vis Spectrometry

UV–vis spectra of gold clusters (prepared as described in Section 2.1.1) and of gold USNPs (prepared as described elsewhere[]) were measured with a Mettler Toledo UV5 Nano Spectrophotometer (Mettler Toledo, Columbus, OH, USA). 3 µL of reaction mixture (medium: Milli-Q water) was dropped on the microvolume platform of the instrument. Spectra were acquired with 120 s long measurements by scanning wavelengths between 200 and 1200 nm.

2.3. Cell Culture

The firefly luciferase-expressing tumor cell-1 (TC-1/Luc) tumor cell line was produced through the infection of the TC-1 cell line, a cancer cell line derived from immortalizing the primary lung cells of C57BL/6 mice with HPV-16 E6 and E7 oncogenes, as well as the human c-Ha-ras oncogene. TC-1/Luc cells were kindly provided by Tzyy-Choou Wu (Johns Hopkins Medical Institutions, Baltimore, MD, USA) in 2009. The cells were cultured in Roswell Park Memorial Institute (RPMI) 1640 medium supplemented with 10% fetal bovine serum (FBS), 1% sodium pyruvate,

1% nonessential amino acids, 1% *N*-(2-hydroxyethyl)piperazine-29-(2-ethane-sulfonic acid), and 1% penicillin/streptomycin. The head and neck murine SCC VII cells were kindly provided by Cornelia Brunner (Universitätsklinik Ulm, Ulm, Germany) and cultured in RPMI-1640 medium supplemented with 10% FBS and 1% penicillin/streptomycin. Normal human dermal fibroblast (nHDF) cells were maintained in a complete growth medium composed by a 1:1 mixture of Dulbecco's modified Eagle's medium and Ham's F12 medium supplemented with 10% FBS, 4 mM L-glutamine, 1 mM sodium pyruvate, 100 U mL^{-1} penicillin, 100 mg mL^{-1} streptomycin (Invitrogen), and 400 ng mL^{-1} hydrocortisone. Cells were maintained at 37 °C in a humidified 5% CO_2 atmosphere.

2.4. Viability Assay

The viability assays were performed by using a water soluble tetrazolium (WST) salt, 2-(2-methoxy-4-nitrophenyl)-3-(4-nitrophenyl)-5-(2,4-disulfophenyl)-2*H* tetrazolium, and monosodium salt assay. TC1/luc, SCC VII, or nHDF cells were seeded in 96-well plate and cultured for 24 h to let the cells adhere. The cells were then incubated in the presence of cisplatin or the nanoarchitectures at increasing concentration in medium (100 µL) for 2 h at 37 °C. After incubation, the drug was removed, and cells were washed twice with PBS and kept in fresh medium. For each experimental time point, cells were incubated with 10% WST reagent (10 µL) and 10% serum-containing medium (90 µL) for 2 h. Absorbance (450 nm) was measured using a microplate reader (Glomax Discovery, Promega, Madison, WI, USA). The percentage/fraction of cell viability was determined by comparing the drug-treated cells with the untreated cells (control, 100% viability).

2.5. Clonogenic Assay

Cells were seeded in 6-well plates with growth medium at a density of 200 cells per well and incubated overnight. The following day, cells were treated with different concentrations of NAs-Cluster (25, 250, and 2500 ng mL^{-1} of gold), NAs-Cluster-CisPt (25, 250, and 2500 ng mL^{-1} of gold), or free cisplatin at a dose equivalent to the amount found in NAs-Cluster-Cisplatin (10, 100, and 1000 ng mL^{-1} of cisplatin) and incubated for 2 h. Subsequently, the cells were washed with fresh medium, incubated for one week, and then fixed and stained with a 0.5% crystal violet solution diluted in ethanol. Colonies consisting of more than 50 cells were counted. The survival fraction (SF) was determined by dividing the plating efficiency (PE) of the treated cells by the PE of the corresponding nontreated cells. PE was calculated by dividing the number of colonies formed by the number of cells seeded in the control dish.

In order to evaluate the radiosensitizer effect of the nanoarchitectures, TC-1/Luc or SCC VII cells were cultured at a density of 200 cells per well in 6-well plates and grown overnight. The following day, cells were treated with NAs-Cluster, NAs-Cluster-CisPt, and free-CisPt (6 ng mL^{-1} of gold and 1.75 ng mL^{-1} of cisplatin) and incubated for 2 h. Then, the cells were washed and incubated with medium. Radiation therapy (RT) treatment was administered 24 h after the application of the nanoarchitectures or the free cisplatin. The cells were irradiated (X-rad 320 kV, 15 mA) with doses of 0, 2, 4, or 8 Gy and maintained for 7 days before staining with a 0.5% crystal violet solution. Survival curves were generated by plotting clonogenic survival against radiation dose and fitted to a linear-quadratic model. The radiosensitization enhancement ratio (ER50) for the drugs (NAs-Cluster-CisPt or free cisplatin) at 50% survival was calculated as follows: ER50 = (dose at 50% survival without the drug)/(dose at 50% survival with the drug).

2.6. In Vivo Experiments

Female C57BL/6 mice (age 7 to 8 weeks) were purchased from Janvier CERT and housed in the Gustave Roussy animal facility. All animal procedures were conducted in compliance with protocols approved by the Ethical Committee CEEA 26 (Gustave Roussy) and followed the recommended guidelines for the proper use and care of laboratory animals. To establish a HNSCC implantation model, syngeneic tumor grafts were initiated at day 0 by injection of 50 µL of PBS suspension containing 0.5×10^6 TC-1/Luc cells at a submucosal site of the right inner lip, as previously described.[22]

Throughout the study, the mice were daily monitored for their health, weight, and behavior. Mice that met predefined criteria, such as tumor size, ulceration, or a loss of more than 20% of their initial weight, were euthanized. The survival time for each treatment group was recorded, starting from the date of tumor challenge until the date of euthanasia for each mouse, in order to perform survival analysis.

2.6.1. Radiosensitization

A total of 45 tumor-bearing mice were randomly divided into 7 groups:

i) control (PBS),
ii) radiation alone (RT),
iii) free cisplatin,
iv) free cisplatin + RT,
v) NAs-Cluster + RT,
vi) NAs-Cluster-CisPt,
vii) NAs-Cluster-CisPt + RT.

Mice in the NAs treatment groups received an intratumoral injection of NAs-Cluster (5 µg Au per mouse diluted in 20 µL sterile PBS) or NAs-Cluster-CisPt (5 µg Au + 1.4 µg CisPt per mouse diluted in 20 µL sterile PBS). The dose of drug in CisPt-treated mice was equivalent to the amount used in the NAs-Cluster-CisPt group.

Mice received single-beam local irradiation to the head and neck region using a 200 kV Varian X-ray irradiator at the total dose of 8 Gy in single fraction 24 h after NP treatment. The irradiation of the tumor grafts was performed by the interposition of a 4 cm thick lead shield. This allowed for selective irradiation of the head and neck region, bearing the tumor.

2.6.2. In Vivo Imaging

To monitor tumor growth, bioluminescence imaging was conducted using the In Vivo Imaging System (IVIS) Lumina III Series (IVIS; Perkin Elmer). Mice were positioned in the supine position within the imaging chamber 10 min after intraperitoneal injection of firefly luciferin (at a dosage of 150 mpk); images were captured while the mice were under sedation through continuous administration of isoflurane (2%). Photographic images and bioluminescence color images were overlaid, and signal quantification was performed using the Living Image Software (Perkin Elmer) and expressed as flux of photons s^{-1}.

2.6.3. Immunohistochemistry

For detection of γH2AX (or phospho-H2AX), a Bond Leïca automated immunostainer instrument was used. Paraffin sections were processed for heat-induced antigen retrieval (ER2 corresponding ethylenediaminetetraacetic acid buffer pH9) for 20 min at 100 °C. Slides were incubated with gamma-H2AX antibody (Cell Signaling #9718, clone 20E3, 1/750) for 60 min at room temperature and detected by Bond Polymer Refine Detection kit. The signal was revealed with 3,3'-diaminobenzidine (DAB) and counterstained with hematoxylin.

Quantification of γH2AX positive cells was performed using the QuPath open software.

2.6.4. ICP-MS

Samples of harvested tumors and organs (liver, spleen) were dried at 80 °C until constant weight was reached, then transferred to glass pressure vials. Acid digestion was performed adding aqua regia while heating at 100 °C. Upon completion, the dried samples were diluted in 2.5 mL of 3% nitric acid solution. Centrifugation was performed to remove solid debris and samples were transferred to 15 mL plastic tubes. Elemental content of gold and platinum was quantified by ICP-MS analysis, as described above (Section 2.2.4).

2.7. Statistical Analyses

The data were reported as mean ± standard deviation (SD). Group comparisons were performed using one-tailed Student's *t*-tests and two-way analysis of variance (ANOVA), as indicated in the figure captions.

For the in vivo biodistribution and tumor growth delay data, mean values, and their corresponding standard errors of the mean were calculated for each group. Differences between groups were evaluated using the Mann–Whitney test.

Regarding the in vivo survival data, the median survival for each group was determined, and differences between groups were assessed using the log-rank test.

Statistical significance was defined as $p < 0.05$. All statistical analyses were conducted using GraphPad Prism software (GraphPad Software Inc., La Jolla, CA).

3. Results and Discussion

3.1. Nanoparticle Synthesis Optimization and Characterization

The optimal design of gold nanoparticles for radiation enhancement has been discussed in several works and it is still under debate since radiosensitization is a complex phenomenon that includes physical, chemical, and biological processes.[23] In general, it is recognized that the radiosensitization efficacy can be improved by carefully modulating the size of the nanoparticle, although no definitive correlation has been yet found.[10] Despite that, there is a certain agreement that a smaller size emphasizes the radiosensitizing effect of gold nanoparticles via a number of mechanisms of both chemical and physical nature.[10,23]

Starting from our standard synthetic protocols to produce hybrid nanoarchitectures, we optimized a new method to synthetize ad hoc NAs for concurrent CRT, named NAs-Cluster. These nanoarchitectures have the typical modular structure of NAs (a silica nanocapsule enclosing polymeric aggregates of gold nanoparticles) where gold USNPs (3 nm diameter) are replaced with gold clusters (1 nm diameter). Gold USNPs are usually synthetized by the reduction of the metal salts (tetrachloroauric acid) via fast addition of sodium borohydride in the presence of poly(sodium 4-styrene sulfonate). To produce NAs-Cluster, reduced GSH was added to the aqueous reaction mixture before tetrachloroauric acid and poly(sodium 4-styrene sulfonate), prior to reduction with sodium borohydride. GSH molecules and gold ions form complexes which act as starters for the nucleation process. This adjunctive step induces the creation of a larger number of nuclei compared to the solution without GSH, yielding smaller USNPs.[12] On this regard, the successful synthesis of gold clusters was demonstrated by the peak broadening in the UV–vis spectrum (Figure S1, Supporting Information). Indeed, this shape is associated to the dominant electronic dephasing mechanism, which involves electron–electron interactions rather than electron–phonon coupling.[24]

As we have already demonstrated, PEI induces an increase in the metal loading of NAs without affecting the biodegradability nor the cytotoxicity of the whole structure.[25] Thus, for the composition of NAs-Cluster, poly(L-lysine) was substituted by PEI for the formation of the polymeric aggregates. Indeed, the NAs-Cluster here reported showed a 25-fold increase in gold content (% w/w) compared to our previously reported gold cluster NAs (0.6% w/w).[12] A scheme of the synthetic procedure for NAs-Cluster is presented in Figure S2 (Supporting Information).

The versatility and simplicity of the standard synthetic procedures have previously allowed to encapsulate various chemical moieties in NAs, including drugs.[18] Here, we successfully applied a similar approach to the new NAs-Cluster by noncovalently loading them with cisplatin (NAs-Cluster-CisPt, **Figure 1**), in order to combine the potential radiosensitizing effect of gold clusters with the intracellular release of the drug. The successful encapsulation of cisplatin was confirmed by ICP-MS analysis (**Table 1**) and by EDX spectroscopy (Figure 1C and Figure S3 (Supporting Information)). The addition of cisplatin did not affect the other features of the nanoarchitectures, such as

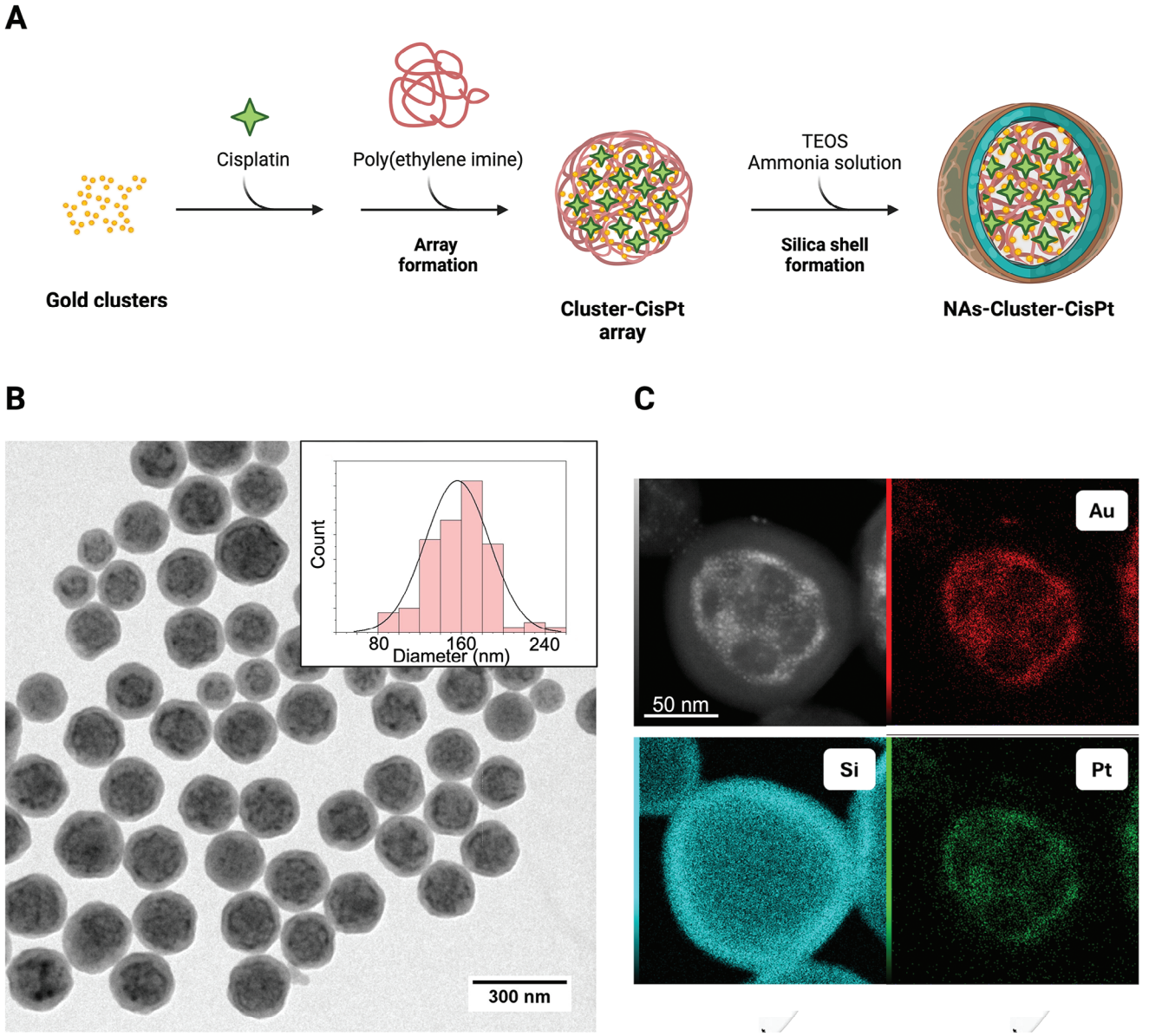

Figure 1. A) Schematic representation of the synthetic protocol for NAs-Cluster-CisPt. B) Transmission electron microscopy (TEM) image of NAs-Cluster-CisPt (scale bar: 300 nm). Inset: distribution of diameters of NAs-Cluster-CisPt measured from TEM images on at least 100 nanoparticles. C) Top left panel: scanning transmission electron microscopy (STEM) image of a single NAs-Cluster-CisPt. Other panels: energy-dispersive X-ray (EDX) spectroscopy map showing the spatial distribution of gold, silicon, and platinum in the nanoarchitecture.

morphology, size, overall charge, shell thickness, and gold content (Table 1 and Figure 1 and Figure S2 (Supporting Information)). Notably, EDX spectroscopy of NAs-Cluster-CisPt demonstrated the encapsulation of both gold and platinum within the polymeric core, while silicon can be found in the shell. It is important to note that, as already demonstrated, the similarity of the overall structure implies comparable physicochemical, biological, and physiological behaviors among the NAs, such as the initial bio-/nanointeractions and nanocapsule biodegradation, while the excretory trends are associated to the nature and the size of the loaded metal.[12,13]

3.2. In Vitro Experiments

The toxicity of the nanoarchitectures was evaluated on TC-1/Luc cells and compared to free cisplatin. TC-1/Luc cells were derived from murine lung epithelial cells that have been transformed with HPV-16 E6 and E7 oncogenes and the human c-Ha-ras oncogene. This genetic manipulation makes TC-1/Luc cells an attractive model for studying HPV-positive cancers. Additionally, TC-1/Luc cells were genetically engineered to express firefly luciferase, enabling noninvasive, real-time monitoring of tumor growth and response to treatments in live animals using bioluminescence imaging. This characteristic is particularly

Table 1. Characteristics of NAs-Cluster, NAs-Cluster-CisPt, and standard NAs. Data are presented as mean ± standard deviation. One-way ANOVA Tukey's multiple comparisons test (*$p \leq 0.05$, **$p \leq 0.01$, ***$p \leq 0.001$, ****$p \leq 0.0001$).

	NAs-Cluster	NAs-Cluster-CisPt	NAs (reproduced from ref. [25])	Statistical analysis		
				NAs-Cluster versus NAs-Cluster-CisPt	NAs-Cluster versus NAs	NAs-Cluster-CisPt versus NAs
Diameter by TEM [nm]	159 ± 37	156 ± 31	108 ± 16	ns	****	****
Shell thickness by TEM [nm]	27.3 ± 4.4	26.0 ± 4.8	18.9 ± 2.2	ns	**	*
Hydrodynamic diameter in PBS by DLS [nm]	299.4 ± 13.3	299.5 ± 7.1	203.1 ± 1.9	ns	****	****
Zeta potential in PBS [mV]	−26.5 ± 1.0	−18.4 ± 0.8	−20.6 ± 0.4	****	***	*
Gold content [%w/w]	14.9 ± 4.6	15.0 ± 7.9	5.9 ± 1.3	ns	Ns	ns
Platinum content [%w/w]	–	3.5 ± 2.6	–	–	–	–

advantageous for assessing the effects of therapeutic strategies in vivo. Furthermore, TC-1/Luc cells can form tumors in immunocompetent syngeneic mice, allowing to investigate tumor progression and immune responses within an in vivo environment, which is essential for evaluating the effectiveness of immunotherapies or radiation treatments.[22,26,27]

TC-1/Luc cells were treated for 2 h with NAs-Cluster and NAs-Cluster-CisPt (25–2500 ng mL^{-1} in gold, 10–1000 ng mL^{-1} in CisPt) or with an equivalent dose of free-CisPt (**Figure 2A**). One week after the treatment, the toxic effect of both NAs-Cluster and NAs-Cluster-CisPt was negligible compared to free cisplatin, as demonstrated by the colony formation. These results were confirmed in the viability/proliferation assay conducted on the TC-1/Luc and SCC VII cells (Figure S4, Supporting Information). The low toxicity profile of both the nanoarchitectures was confirmed on 2D cultured human dermal fibroblast, whose viability and proliferation were not significantly affected by the nanoarchitectures (Figure S5, Supporting Information). These data allowed to calibrate the ideal doses of gold and cisplatin (6 and 1.75 ng mL^{-1}, respectively) for the following investigations on combined CRT to avoid saturation effects of the chemotherapy over radiotherapy. The effects of radiation in combination with NAs-Cluster-CisPt on the clonogenic potential of TC1/Luc cells were evaluated by colony forming assays and compared, as controls, to NAs-Cluster and free-CisPt.[28] The radiosensitizing effects of the nanoarchitectures were evaluated at increasing radiation doses (0, 2, 4, or 8 Gy) of 320 keV photon beams (Figure 2B). RT treatment was administered 24 h after the incubation with the nanoarchitectures, i.e., after their biodegradation, in agreement with Cassano et al.[29] Data were normalized over the nontreated nor irradiated controls, to evaluate the intrinsic toxicity of the treatments. As expected, we observed a promising reduction in the SF of the cells for all the combined treatments with respect to RT alone, especially for the NAs-Cluster-CisPt/RT group. We then performed the same experimental approach described in Figure S6 (Supporting Information) to evaluate the response of a HPV-negative HNSCC cell line (SCC VII cells) to the nanoarchitectures. The colony forming assay showed that, when tested in combination with RT, NAs-Cluster-CisPt strongly reduced the SF of SCC VII cells at a similar extent to the one induced by the CisPt treatment (Figure S7, Supporting Information).

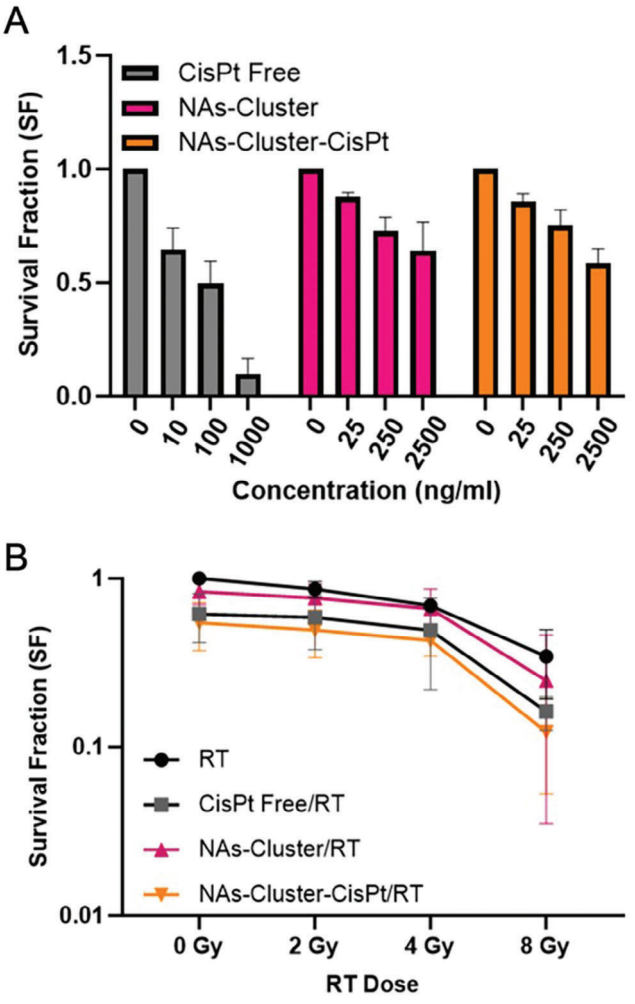

Figure 2. A) Clonogenic assay with different concentrations of NAs-Cluster, NAs-Cluster-CisPt, and free cisplatin. The gold concentration in NAs-Cluster and in NAs-Cluster-CisPt is specified, while the concentration of free cisplatin is equivalent to the amount found in NAs-Cluster-CisPt. B) Survival curves of TC1/Luc cells treated with NAs-Cluster, NAs-Cluster-CisPt, or free-CisPt (6 ng mL^{-1} in gold, 1.75 ng mL^{-1} in platinum) and irradiated at the indicated dose 24 h after the treatment. Each in vitro experiment was conducted thrice, with duplicate or triplicate samples.

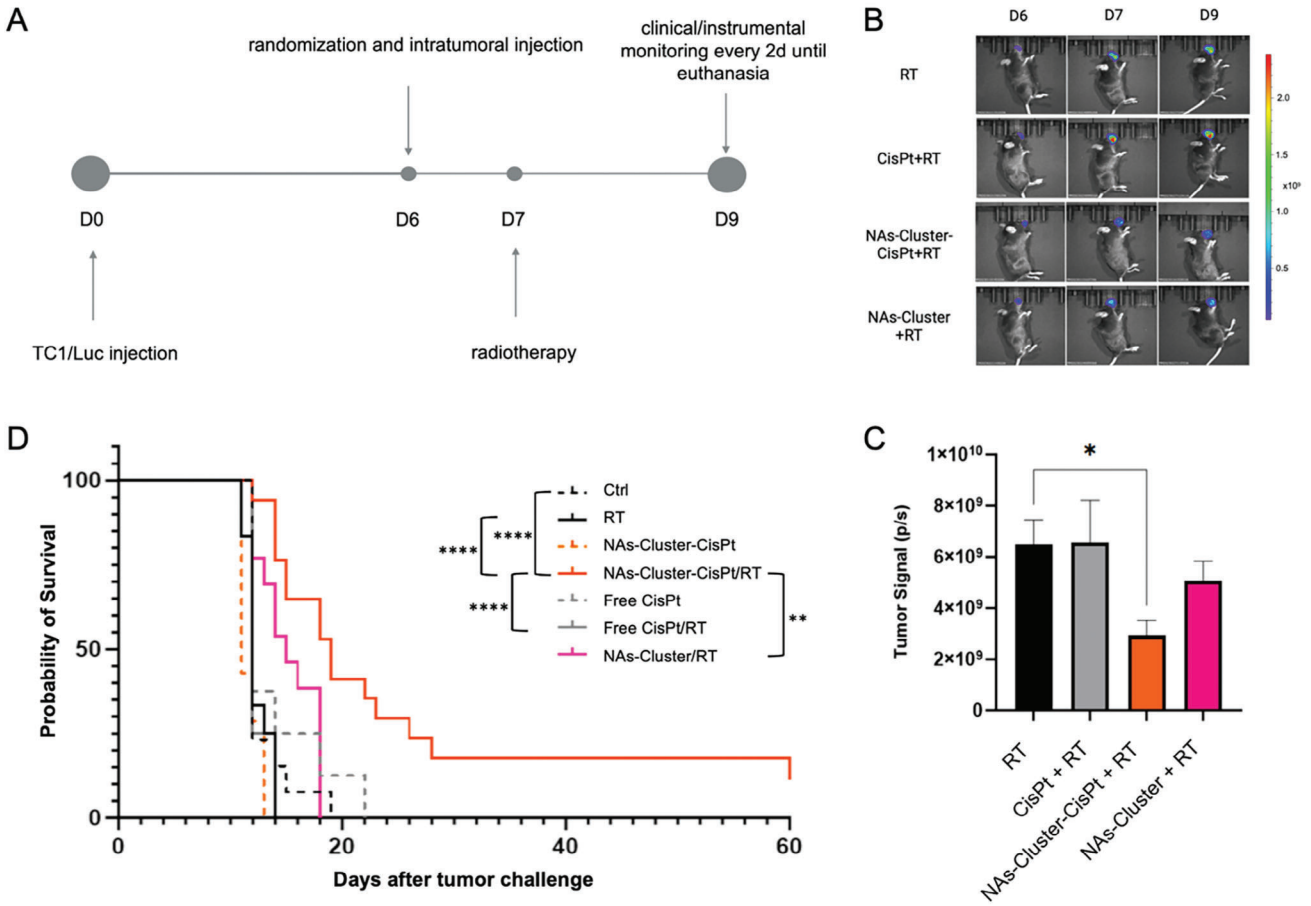

Figure 3. A) Experimental setup. On day 6, mice were randomized and divided in seven groups for intratumoral administration of PBS (control), free cisplatin, NAs-Cluster, and NAs-Cluster-CisPt. Radiotherapy was delivered at day 7. Tumor measurements were recorded every 2 days until death. B) Bioluminescent imaging was conducted every two days to monitor tumor growth. Representative images taken at days 6, 7, and 9 are shown. C) Quantification of the bioluminescent signal was performed at day 9. Data are reported as mean ± SD, with at least 7 mice per treatment group. *$p <$ 0.05, determined by one-way ANOVA followed by Dunnett's post-test for comparing tumor sizes at day 9. D) Survival curves. Kaplan–Meier survival curves of the models. **** $p < 0.0001$; ** $p < 0.01$; log-rank test.

These findings agreeing with other in vitro studies aimed to explore the effects of standard gold NPs on HNSCCs. For example, Teraoka et al. demonstrated that gold NPs can increase the effectiveness of radiation therapy by enhancing the cytotoxic effect on human head and neck cancer cells through the induction of apoptosis.[30] Similar results were found by Zheng and Sanche, who explored the synergistic effects of gold NPs in combination with anticancer drugs and radiation.[31] However, despite the documented in vitro efficacy, significant discrepancies are present among the studies in some critical parameters, such as the cell line, radiation energy, physicochemical attributes of the gold NPs (size and shape), NP concentration, and the duration of incubation.[32] On the other hand, some consistent findings have emerged, such as the critical role of the cellular localization of NPs associated to their size.[23] On this regard, gold nanoparticles demonstrated an improved distribution to key subcellular compartments for X-ray sensitization, such as the nucleus, by reducing the size.[33]

3.3. In Vivo Experiments

On this basis, we further evaluated the radiosensitizing effects of NAs-Cluster and NAs-Cluster-CisPt on an immunocompetent orthotopic murine model of head and neck cancer. The model was obtained by engrafting HPV16 E7-expressing TC-1/Luc cells at the submucosal site of the inner lip in C57BL/6 mice. This model has been extensively used by us and others to mimic a HPV-positive head and neck tumor.[22,26,27] The treatment protocol was designed by combining local tumor irradiation (IR) with intratumoral administration of NAs-Cluster, NAs-Cluster-CisPt, free-CisPt, or PBS (**Figure 3A**).

The intratumoral injection was preferred in agreement with recent running trials and clinical evaluations of radiosensitizing hafnium oxide nanoparticles for patients' treatment of locally advanced head and neck cancer or soft-tissue sarcoma.[34,35] The amount of gold and/or platinum for the tested treatments was fixed at, respectively, 5 and 1.4 µg by following the previous in vitro assays, our earlier experience on ADMET evaluation of the

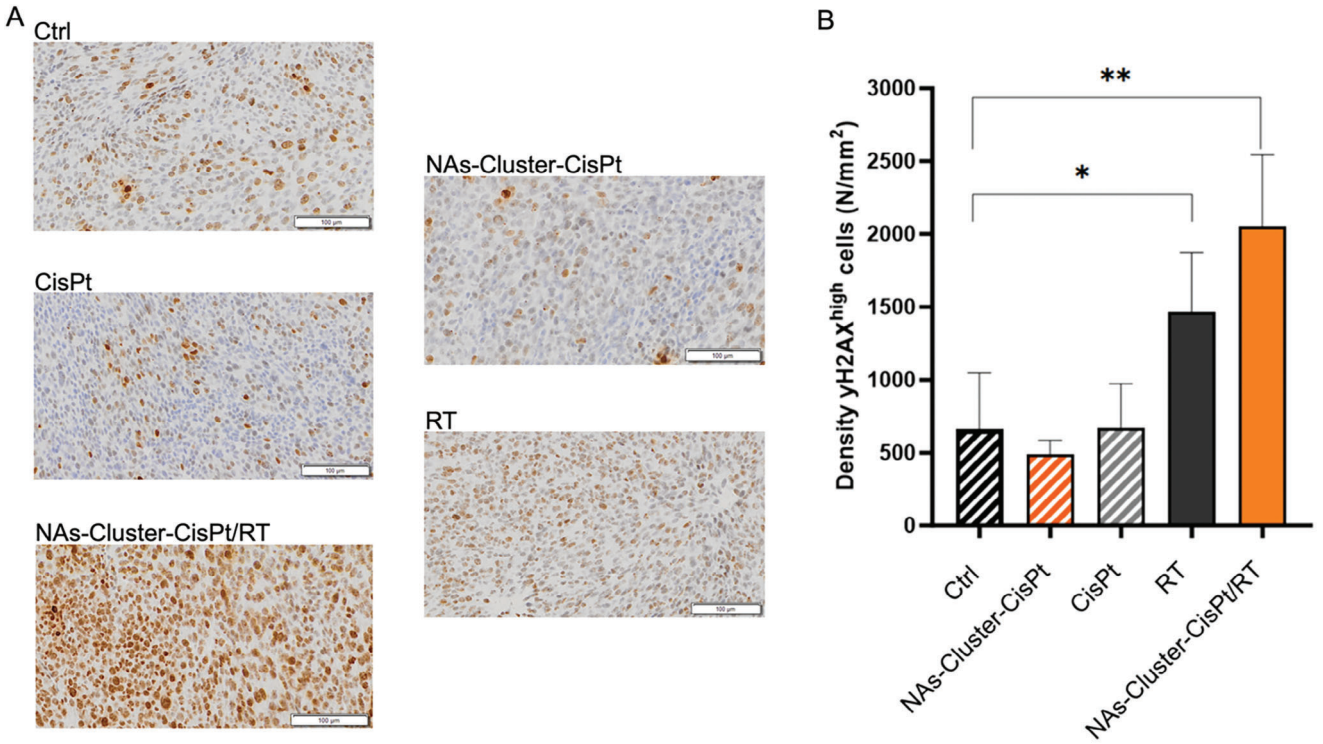

Figure 4. A) Representative IHC images. Staining with anti γH2AX was performed 1 h after irradiation. Scale bars = 100 µm. B) IHC images were analyzed with QuPath software for quantitative evaluation of cells displaying high levels of γH2AX (γH2AX^{high}-positive cells), as a biomarker of double strand breaks DSB. Data are reported as mean ± SD, with at least 3 mice per treatment group. Statistical differences were calculated with one-way ANOVA followed by Tukey's multiple comparisons test, *$p < 0.05$, ** $p < 0.01$.

nanoarchitectures, and the concentration of gold required for radiosensitization effects (0.1 mg mL^{-1}).[12,36] In agreement with our previous investigations, we opted for a single high dose RT (8 Gy).[22,37] Indeed, other in vivo studies have evaluated the radiosensitization effects of NPs under external beam RT (5–30 Gy) in order to achieve an evident tumor response.[23] As expected, mice receiving the combined CRT exhibited significantly smaller tumor burden compared to those treated with monomodal therapies (RT, nanoarchitectures, or free-CisPt). Mice treated with the NAs-Cluster-CisPt/RT combination demonstrated a significant reduction in tumor signal (Figure 3B,C and Figures S8 and S9 (Supporting Information)) and a substantial increase in survival (Figure 3D) compared to the control groups. Remarkably, 25% of the mice treated with the NAs-Cluster-CisPt/RT combination achieved a complete tumor clearance that persisted throughout the 60 days observation period (Figure 3D). This result is promising, as only a limited number of studies report the in vivo effectiveness of gold nanomaterials as radiosensitizers in HNSCC models and even less with nonpersistent materials.[38–40]

To preliminarily explore the mechanistic role of the NAs-Cluster-CisPt in the increased antitumor efficacy of RT, we evaluated the extent of tumor DNA damage ex vivo after the different treatments by performing immunohistochemical (IHC) staining to detect the phosphorylated form of the histone protein H2AX (γH2AX) as a biomarker of DNA damage. As expected, irradiation induced a strong increase of γH2AX signal (**Figure 4A**) even at a reduced irradiation beam (2 Gy). Interestingly, the staining was even higher when mice were treated with NAs-Cluster-CisPt 24 h before RT. In agreement, the quantification of cells displaying high γH2AX signal (γH2AX^{high} cells) showed a significant increase for RT-treated tumors compared to the control ones (Figure 4B and $p < 0.05$). Of note, such density was further increased in mice treated with the combination of NAs-Cluster-CisPt and RT (Figure 4B and $p < 0.01$). These results suggest that an increased DNA damage may contribute to the observed antitumor efficacy of NAs-Cluster-CisPt when combined with RT.

ICP-MS was performed to detect the amount of gold and platinum that persisted in the liver and spleen 20 days and 6 months after the treatment with NAs-Cluster-CisPt (Figure S10, Supporting Information). These organs were selected for metal persistence quantification, as the accumulation of xenobiotics is generally high and associated with the uptake by hepatic and splenic macrophages.[41] As expected, the favorable excretion trend of the gold loaded in the nanoarchitectures was further confirmed. Indeed, a negligible amount of the metal was found in these organs as the cluster-sized gold NPs contained in NAs can be efficiently excreted by the renal pathway (60% of the injected dose in cumulative excretions in 10 days) without damaging the kidneys.[12]

4. Conclusions

In conclusion, this study presents a promising strategy to improve the treatment outcome in locally advanced HPV+ HNSCC patients. Our findings highlight the potential of combining

NAs-Cluster-CisPt with local radiotherapy and corroborate the evidence of the critical role that rationally designed gold nanomaterials may play in improving radio-oncology treatments by increasing the tumor sensitivity to radiation while sparing healthy tissue. In this regard, it is worth to notice that the NAs are pioneering nanomaterials designed to jointly combine the features of noble metal nanomaterials with optimal excretion trends, making them able to avoid one of the main concerns that prevented the clinical translation of nanostructured gold, the persistence issue.[11] The intratumoral injection of NAs may represent a limitation that can be overcome by decorating the nanoarchitectures with targeting agents, such as transferrin recognizing peptides, supporting for an intravenous delivery.[42] The next step should involve evaluating the potential of NAs-Cluster-CisPt as radiosensitizers in combination with fractionated RT.[43] However, this study represents the very first reporting in vitro and in vivo assessment of the combination of excretable noble metal nanomaterials and radiotherapy on immunocompetent HPV+ models of HNSCC. Overall, our findings indicate that NAs-Cluster-CisPt represent a promising candidate to expand the therapeutic window in oral cancer management mediated by nonpersistent metal nanomaterials.

Supporting Information

Supporting Information is available from the Wiley Online Library or from the author.

Acknowledgements

This work was supported by the MFAG 2017 – ID 19852 from the Associazione Italiana per la Ricerca sul Cancro (AIRC) granted to V.V., by INSERM, SIRIC SOCRATE and the Institut National du Cancer (INCa, Project No. SEQ-RTH22-014) to E.D. and M.M. The authors thank the staff of the animal facilities at the Gustave Roussy for their invaluable expertise, and Patrick Gonin and Karine Ser-Le-Roux at the Pre-clinical Evaluation platform (PFEP) at the Gustave Roussy. The authors thank the Center for Instrument Sharing of the University of Pisa (CISUP).

Conflict of Interest

C.C., L.M., E.D., and M.M. declare grants from the Roche Genentech, AstraZeneca, Merck Serono, Bristol Myers Squibb, Boehringer Ingelheim, and MSD, outside the submitted work. E.D. declares consulting fees from Graegis. All the other authors declare no conflict of interest.

Author Contributions

A.G., M.G.d.T., and M.L.E. contributed equally to this work. F.P., M.M. and V.V. share the senior authorship. A.G., M.G.d.T., M.M.: in vivo experiments; A.G., M.G.d.T., I.E.-A., and N.G.: in vitro experiments; A.G., M.L.E., and V.F.: nanoarchitecture synthesis and characterizations; G.D.: ICP measurements; E.M.: TEM measurements; P.S.: data analysis; N.S., O.B., C.C., L.M., and P.B.: histological evaluations; E.D., F.P., M.M., and V.V.: data interpretation; M.M., V.V.: design and coordination. All the authors have discussed the data and contributed to writing the paper.

Data Availability Statement

The data that support the findings of this study are available from the corresponding author upon reasonable request.

Keywords

chemoradiotherapy, combined therapy, gold nanoparticles, head and neck carcinoma, radiosensitization

Received: January 18, 2024
Revised: May 13, 2024
Published online: May 27, 2024

[1] C. Fakhry, W. H. Westra, S. Li, A. Cmelak, J. A. Ridge, H. Pinto, A. Forastiere, M. L. Gillison, *J. Natl. Cancer Inst.* **2008**, *100*, 261.
[2] D. E. Johnson, B. Burtness, C. R. Leemans, V. W. Y. Lui, J. E. Bauman, J. R. Grandis, *Nat. Rev. Dis. Primers* **2020**, *6*, 92.
[3] P. Strojan, K. A. Hutcheson, A. Eisbruch, J. J. Beitler, J. A. Langendijk, A. W. M. Lee, J. Corry, W. M. Mendenhall, R. Smee, A. Rinaldo, A. Ferlito, *Cancer Treat. Rev.* **2017**, *59*, 79.
[4] H. Mirghani, F. Amen, P. Blanchard, F. Moreau, J. Guigay, D. M. Hartl, J. Lacau St Guily, *Int. J. Cancer* **2015**, *136*, 1494.
[5] H. Mehanna, M. Robinson, A. Hartley, A. Kong, B. Foran, T. Fulton-Lieuw, M. Dalby, P. Mistry, M. Sen, L. O'Toole, H. Al Booz, K. Dyker, R. Moleron, S. Whitaker, S. Brennan, A. Cook, M. Griffin, E. Aynsley, M. Rolles, E. De Winton, A. Chan, D. Srinivasan, I. Nixon, J. Grumett, C. R. Leemans, J. Buter, J. Henderson, K. Harrington, C. McConkey, A. Gray, et al., *Lancet* **2019**, *393*, 51.
[6] M. L. Gillison, A. M. Trotti, J. Harris, A. Eisbruch, P. M. Harari, D. J. Adelstein, E. M. Sturgis, B. Burtness, J. A. Ridge, J. Ringash, J. Galvin, M. Yao, S. A. Koyfman, D. M. Blakaj, M. A. Razaq, A. D. Colevas, J. J. Beitler, C. U. Jones, N. E. Dunlap, S. A. Seaward, S. Spencer, T. J. Galloway, J. Phan, J. J. Dignam, Q. T. Le, *Lancet* **2019**, *393*, 40.
[7] P. Golusinski, J. Corry, V. Vander Poorten, R. Simo, E. Sjögren, A. Mäkitie, L. P. Kowalski, J. Langendijk, B. J. M. Braakhuis, R. P. Takes, A. Coca-Pelaz, J. P. Rodrigo, S. M. Willems, A. A. Forastiere, R. De Bree, N. F. Saba, Y. Teng, A. Sanabria, P. Di Maio, M. Szewczyk, A. Ferlito, *Oral Oncol.* **2021**, *123*, 105620.
[8] L. Gong, Y. Zhang, C. Liu, M. Zhang, S. Han, *Int. J. Nanomed.* **2021**, *16*, 1083.
[9] M. Haque, M. S. Shakil, K. M. Mahmud, *Cancers* **2023**, *15*, 1892.
[10] S. Penninckx, A. C. Heuskin, C. Michiels, S. Lucas, *Cancers* **2020**, *12*, 2021.
[11] D. Cassano, S. Pocoví-Martínez, V. Voliani, *Bioconjugate Chem.* **2018**, *29*, 4.
[12] D. Cassano, A. K. Mapanao, M. Summa, Y. Vlamidis, G. Giannone, M. Santi, E. Guzzolino, L. Pitto, L. Poliseno, R. Bertorelli, V. Voliani, *ACS Appl. Bio Mater.* **2019**, *2*, 4464.
[13] D. Cassano, M. Summa, S. Pocoví-Martínez, A. K. Mapanao, T. Catelani, R. Bertorelli, V. Voliani, *Part. Part. Syst. Charact.* **2019**, *36*, 1800464.
[14] A. Zamborlin, M. L. Ermini, M. Summa, G. Giannone, V. Frusca, A. K. Mapanao, D. Debellis, R. Bertorelli, V. Voliani, *Nano Lett.* **2022**, *22*, 5269.
[15] A. K. Mapanao, G. Giannone, M. Summa, M. L. Ermini, A. Zamborlin, M. Santi, D. Cassano, R. Bertorelli, V. Voliani, *Nanoscale Adv.* **2020**, *2*, 3815.
[16] A. Zamborlin, P. Sarogni, V. Frusca, A. Gonnelli, N. Giannini, M. L. Ermini, A. Marranci, F. Pagliari, C. M. Mazzanti, J. Seco, V. Voliani, *ACS Appl. Nano Mater.* **2023**, *6*, 22532.
[17] D. Cassano, M. Santi, F. D'Autilia, A. K. Mapanao, S. Luin, V. Voliani, *Mater. Horiz.* **2019**, *6*, 531.
[18] A. K. Mapanao, M. Santi, V. Voliani, *J. Colloid Interface Sci.* **2021**, *582*, 1003.

[19] P. P. Che, A. K. Mapanao, A. Gregori, M. L. Ermini, A. Zamborlin, M. Capula, D. Ngadimin, B. J. Slotman, V. Voliani, P. Sminia, E. Giovannetti, *Cancers* **2022**, *14*, 3034.
[20] C. Avigo, D. Cassano, C. Kusmic, V. Voliani, L. Menichetti, *J. Phys. Chem. C* **2017**, *121*, 6955.
[21] A. Gonnelli, P. Sarogni, N. Giannini, S. Linsalata, F. Di Martino, A. Zamborlin, V. Frusca, M. L. Ermini, P. Puccini, V. Voliani, F. Paiar, *Artif. Cells, Nanomed., Biotechnol.* **2024**, *52*, 122.
[22] M. Mondini, M. Nizard, T. Tran, L. Mauge, M. Loi, C. Clémenson, D. Dugue, P. Maroun, E. Louvet, J. Adam, C. Badoual, D. Helley, E. Dransart, L. Johannes, M. C. Vozenin, J. L. Perfettini, E. Tartour, E. Deutsch, *Mol. Cancer Ther.* **2015**, *14*, 1336.
[23] Y. Chen, J. Yang, S. Fu, J. Wu, *Int. J. Nanomed.* **2020**, *15*, 9407.
[24] D. M. Pashkov, A. A. Guda, M. V. Kirichkov, S. A. Guda, A. Martini, S. A. Soldatov, A. V. Soldatov, *J. Phys. Chem. C* **2021**, *125*, 8656.
[25] G. Giannone, M. Santi, M. L. Ermini, D. Cassano, V. Voliani, *Nanomaterials* **2020**, *10*, 1600.
[26] F. Sandoval, M. Terme, M. Nizard, C. Badoual, M. F. Bureau, L. Freyburger, O. Clement, E. Marcheteau, A. Gey, G. Fraisse, C. Bouguin, N. Merillon, E. Dransart, T. Tran, F. Quintin-Colonna, G. Autret, M. Thiebaud, M. Suleman, S. Riffault, T. C. Wu, O. Launay, C. Danel, J. Taieb, J. Richardson, L. Zitvogel, W. H. Fridman, L. Johannes, E. Tartour, *Sci. Transl. Med.* **2013**, *5*, 172ra20.
[27] P. Hamon, M. Gerbé De Thoré, M. Classe, N. Signolle, W. Liu, O. Bawa, L. Meziani, C. Clémenson, F. Milliat, E. Deutsch, M. Mondini, *J. Immunother. Cancer* **2022**, *10*, e003519.
[28] N. A. P. Franken, H. M. Rodermond, J. Stap, J. Haveman, C. van Bree, *Nat. Protoc.* **2006**, *1*, 2315.
[29] D. Cassano, M. Santi, V. Cappello, S. Luin, G. Signore, V. Voliani, *Part. Part. Syst. Charact.* **2016**, *33*, 818.
[30] S. Teraoka, Y. Kakei, M. Akashi, E. Iwata, T. Hasegawa, D. Miyawaki, R. Sasaki, T. Komori, *Biomed. Rep.* **2018**, *9*, 415.
[31] Y. Zheng, L. Sanche, *Radiat. Res.* **2009**, *172*, 114.
[32] N. Bloise, S. Strada, G. Dacarro, L. Visai, *Int. J. Mol. Sci.* **2022**, *23*, 7683.
[33] K. Huang, H. Ma, J. Liu, S. Huo, A. Kumar, T. Wei, X. Zhang, S. Jin, Y. Gan, P. C. Wang, S. He, X. Zhang, X. J. Liang, *ACS Nano* **2012**, *6*, 4483.
[34] S. Bonvalot, P. L. Rutkowski, J. Thariat, S. Carrère, A. Ducassou, M. P. Sunyach, P. Agoston, A. Hong, A. Mervoyer, M. Rastrelli, V. Moreno, R. K. Li, B. Tiangco, A. C. Herraez, A. Gronchi, L. Mangel, T. Sy-Ortin, P. Hohenberger, T. de Baère, A. Le Cesne, S. Helfre, E. Saada-Bouzid, A. Borkowska, R. Anghel, A. Co, M. Gebhart, G. Kantor, A. Montero, H. H. Loong, R. Vergés, et al., *Lancet Oncol.* **2019**, *20*, 1148.
[35] X. Liem, T. De Baere, T. Y. Seiwert, C. Shen, Z. Papai, V. Moreno, Z. Takacsi-Nagy, F. Helferich, J. O. Thariat, Z. Gooi, O. I. Vivar, L. A. Farber, S. S. Yom, P. Bossi, R. L. Ferris, T. Hackman, C. Le Tourneau, J. Rodriguez, C. Hoffmann, *Int. J. Radiat. Oncol., Biol., Phys.* **2022**, *114*, e310.
[36] A. Al Zaki, D. Joh, Z. Cheng, A. L. B. De Barros, G. Kao, J. Dorsey, A. Tsourkas, *ACS Nano* **2014**, *8*, 104.
[37] M. Mondini, P. L. Loyher, P. Hamon, M. G. de Thore, M. Laviron, K. Berthelot, C. Clemenson, B. L. Salomon, C. Combadiere, E. Deutsch, A. Boissonnas, *Cancer Immunol. Res.* **2019**, *7*, 376.
[38] O. Piccolo, J. D. Lincoln, N. Melong, B. C. Orr, N. R. Fernandez, J. Borsavage, J. N. Berman, J. Robar, M. N. Ha, *Sci. Rep.* **2022**, *12*, 1559.
[39] P. Dubey, M. Sertorio, V. Takiar, *Cancers* **2022**, *14*, 514.
[40] A. Popovtzer, A. Mizrachi, M. Motiei, D. Bragilovski, L. Lubimov, M. Levi, O. Hilly, I. Ben-Aharon, R. Popovtzer, *Nanoscale* **2016**, *8*, 2678.
[41] H. H. Gustafson, D. Holt-Casper, D. W. Grainger, H. Ghandehari, *Nano Today* **2015**, *10*, 487.
[42] A. K. Mapanao, P. Sarogni, M. Santi, M. Menicagli, A. Gonnelli, A. Zamborlin, M. L. Ermini, V. Voliani, *Biomater. Sci.* **2022**, *10*, 6135.
[43] M. Y. Chang, A. L. Shiau, Y. H. Chen, C. J. Chang, H. H. W. Chen, C. L. Wu, *Cancer Sci.* **2008**, *99*, 1479.